Kinetic and Structural Characterization of Manganese(II)−Loaded Methionyl Aminopeptidases †

ARTICLE *in* BIOCHEMISTRY · NOVEMBER 2002

Impact Factor: 3.02 · DOI: 10.1021/bi020395u · Source: PubMed

Kinetic and Structural Characterization of Manganese(II)-Loaded Methionyl Aminopeptidases†

Ventris M. D'souza,‡ Sabina I. Swierczek,‡ Nathaniel J. Cosper,§ Lu Meng,‡ Shane Ruebush,‡ Alicja J. Copik,‡ Robert A. Scott,*,§ and Richard C. Holz*,‡

Department of Chemistry and Biochemistry, Utah State University, Logan, Utah 84322-0300, and Department of Chemistry, University of Georgia, Athens, Georgia 30602-2556

Received May 31, 2002; Revised Manuscript Received August 9, 2002

ABSTRACT: Manganese(II) activation of the methionyl aminopeptidases from *Escherichia coli* (*Ec*MetAP-I) and the hyperthermophilic archaeon *Pyrococcus furiosus* (*Pf*MetAP-II) was investigated. Maximum catalytic activity for both enzymes was obtained with 1 equiv of Mn(II), and the dissociation constants (K_d) for the first metal binding site were found to be 6 ± 0.5 and 1 ± 0.5 μM for *Ec*MetAP-I and *Pf*MetAP-II, respectively. These K_d values were verified by isothermal titration calorimetry (ITC) and found to be 3.0 ± 0.2 and 1.4 ± 0.2 μM for *Ec*MetAP-I and *Pf*MetAP-II, respectively. The hydrolysis of MGMM was measured in triplicate between 25 and 85 °C at eight substrate concentrations ranging from 2 to 20 mM for *Pf*MetAP-II. Both specific activity and K_m values increased with increasing temperature. An Arrhenius plot was constructed from the k_{cat} values and was found to be linear over the temperature range 25−85 °C. The activation energy for the Mn(II)-loaded *Pf*MetAP-II hydrolysis of MGMM was found to be 25.7 kJ/mol while the remaining thermodynamic parameters calculated at 25 °C are $\Delta G^{\ddagger} = 50.1$ kJ/mol, $\Delta H^{\ddagger} = 23.2$ kJ/mol, and $\Delta S^{\ddagger} = -90.2$ J·mol^{-1}·K^{-1}.

Methionyl aminopeptidases (MetAP's)[1] represent a unique class of proteases that are capable of the hydrolytic removal of N-terminal methionine residues from nascent polypeptide chains (*1*−*4*). The biosynthesis of all eukaryotic proteins present in the cytosol is initiated with methionine, while in prokaryotes, mitochondria, and chloroplasts, the initiator residue is an *N*-formylmethionine group. The *N*-formyl group is removed from proteins in prokaryotes and eukaryotic organelles by a deformylase, leaving a methionine residue at the amino terminus (*2*). Subsequently, the N-terminal methionine is cleaved by MetAP. While the rationale for the removal of the initiator methionine remains unclear, several explanations have been proposed (*5*). Some involve the facilitation of further processing after excision of N-terminal groups such as the removal of signal sequences, proteolytic cleavage to generate shorter peptides, and the covalent attachment of residues and blocking groups such as acetyl and myristoyl groups (*4*). The structure of the mature N-terminus plays a role in N-directed degradation pathways (*3*, *6*) and in targeting to cellular membranes (*1*−*4*). MetAP's are therefore one of the key cellular enzymes involved in protein maturation. The physiological importance of MetAP activity is underscored by the lethality of the deletion of the genes in *Escherichia coli*, *Salmonella typhimurium*, and *Saccharomyces cerevisiae* (*7*−*9*). For this reason, MetAP's are under intense scrutiny as potential targets for antibacterial and antifungal drugs.

MetAP's are organized into two classes (types I and II) on the basis of the absence or presence of an extra 62 amino acid sequence (of unknown function) inserted near the catalytic domain. The type I MetAP from *E. coli* (*Ec*MetAP-I) and the type II MetAP's from *Homo sapiens* (*Hs*MetAP-II) and *Pyrococcus furiosus* (*Pf*MetAP-II) have been crystallographically characterized (*10*−*13*). All of these MetAP's have identical catalytic domains that contain a bis(μ-carboxylato)(μ-aquo/hydroxo)dicobalt core with an additional carboxylate residue at each metal site and a single histidine residue bound to one of the two metal ions (*10*−*13*). Each structure also revealed the presence of two solvent molecules in the active site, one of which bridges the two Co(II) ions while the second acts as a terminal ligand coordinated to the non-histidine-ligated Co(II) ion. In all three structures, both Co(II) ions appear to reside in a trigonal-bipyramidal coordination environment (*10*−*13*). Since all of the catalytic domain residues are completely conserved for both type I and type II MetAP's, all MetAP's likely bind divalent metal ions in a similar fashion. This suggestion was recently verified by comparison of the divalent metal binding properties of *Ec*MetAP-I and *Pf*MetAP-II (*14*, *15*).

Until recently, all MetAP's studied had been reported to be Co(II)-dependent metalloproteases (*16*, *17*). While the identity of the in vivo metal ion has not been established for any MetAP, Fe(II) and Mn(II) were suggested as potential

† This work was supported by the National Institutes of Health (GM-56495, R.C.H.; GM-42025, R.A.S.).

* To whom correspondence should be addressed. R.C.H.: phone, (435) 797-2609; fax, (435) 797-3390; e-mail, rholz@cc.usu.edu.

‡ Utah State University.

§ University of Georgia.

[1] Abbreviations: MetAP, methionyl aminopeptidase; Hepes, *N*-(2-hydroxyethyl)piperazine-*N*′-2-ethanesulfonic acid; MAS, tripeptide Met-Ala-Ser; MGMM, tetrapeptide Met-Gly-Met-Met; EPR, electron paramagnetic resonance; EXAFS, extended X-ray absorption fine structure; XAS, X-ray absorption spectroscopy; ICP-AES, inductively coupled plasma−atomic emission spectroscopy; NMR, nuclear magnetic resonance.

10.1021/bi020395u CCC: $22.00
Published on Web 10/04/2002

candidates on the basis of whole cell metal analyses for *Ec*MetAP-I (*18*). Further studies on Co(II) and Fe(II) binding to *Ec*MetAP-I and *Pf*MetAP-II led to the proposal that MetAP's function as mononuclear enzymes in vitro (*14*, *15*). Structural evidence for a mononuclear Co(II) or Fe(II) active site in MetAP's was recently obtained by use of extended X-ray absorption fine structure (EXAFS) (*19*). The high-affinity or catalytically relevant metal binding site was assigned as the histidine-containing side of the active site on the basis of EXAFS and ^{1}H NMR data (*15*). Mn(II) was also shown to activate *Ec*MetAP-I, but no kinetic or structural information has been reported. Herein, we report the catalytic and structural properties of the Mn(II)-loaded forms of both *Ec*MetAP-I and *Pf*MetAP-II. On the basis of kinetic, thermodynamic, and EXAFS data, Mn(II) is shown to bind to both type I and type II MetAP's in a fashion similar to that of Co(II) and Fe(II). Because *Pf*MetAP-II and *Hs*MetAP-II are 39% identical while *Pf*MetAP-II and *Ec*MetAP-I are 33% identical, the structural and mechanistic data obtained for the Mn(II)-loaded *Ec*MetAP-I and *Pf*MetAP-II can be extrapolated to *Hs*MetAP-II. The catalytic and structural similarities and differences between Co(II)- and Mn(II)-loaded MetAP's are also discussed.

MATERIALS AND METHODS

Purification of MetAP Enzymes. All chemicals used in this study were purchased commercially and were of the highest quality available. Recombinant *Ec*MetAP-I was expressed and purified as an apoenzyme, as previously described, from a stock culture kindly provided by Drs. Brian W. Matthews and W. Todd Lowther (*18*, *20*). The as purified *Ec*MetAP-I exhibited a single band on SDS−PAGE. Protein concentrations were obtained spectrophotometrically at 280 nm using an extinction coefficient ϵ_{280} of 16445 M^{-1} cm^{-1} (*18*, *20*). Apo-*Ec*MetAP-I was washed free of methionine using Chelex-treated methionine-free buffer (25 mM Hepes, pH 7.5, 150 mM KCl) and concentrated by microfiltration using a Centrocon-10 (Amicon, Beverly, MA) prior to all kinetic assays. Individual aliquots of apo-EcMetAP-I were routinely stored at −80 °C or in liquid nitrogen until needed.

*Pf*MetAP-II was purified as previously reported (*14*). Purified *Pf*MetAP-II exhibited a single band on SDS−PAGE with a M_r of 32800. Protein concentrations were estimated from the absorbance at 280 nm using an extinction coefficient of 21650 M^{-1} cm^{-1}. Metal-free *Pf*MetAP-II was prepared by concentrating the as purified *Pf*MetAP-II to a volume of ∼5 mL after which EDTA was added to a final concentration of 10 mM. The resulting protein solution was dialyzed against 25 mM Hepes buffer (2 L, pH 7.5) containing 10 mM EDTA and 150 mM KCl at 4 °C for 2 days with two buffer changes per day. The protein solution was then dialyzed against chelexed (Chelex-100 column) 25 mM Hepes buffer (2 L, pH 7.5) containing 150 mM KCl for 3 days against two buffer changes per day. The resulting *Pf*MetAP-II was inactive and was found to contain no detectable metal ions via inductively coupled plasma-atomic emission spectrometry (ICP-AES). This enzyme deemed "apo-*Pf*MetAP-II" was stored at −80 °C.

Metal Content Measurements. *Ec*MetAP-I and *Pf*MetAP-II samples used for metal analysis were typically 30 μM. Apo-*Ec*MetAP-I or apo-*Pf*MetAP-II samples were incubated under anaerobic conditions with Mn(II) ($MnCl_2$ = 99.999%; Strem Chemicals, Newburyport, MA, or Aldrich) for 30 or 90 min, respectively, prior to exhaustive dialysis under anaerobic conditions against Chelex-treated buffer as previously reported (*15*, *18*). Metal analyses were performed using ICP-AES.

Enzymatic Assay of MetAP's. All enzymatic assays were performed under strict anaerobic conditions in an inert atmosphere glovebox (Coy) with a dry bath incubator to maintain the temperature. Catalytic activities were determined with an error of ±5%. Enzyme activities for both *Ec*MetAP-I and *Pf*MetAP-II were determined in 25 mM Hepes buffer, pH 7.5, containing 150 mM KCl with the tri- or tetrapeptide substrates MAS or MGMM, respectively. The amount of product formation was determined by high-performance liquid chromatography (HPLC, Shimadzu LC-10A class-VP5). A typical assay involved the addition of 4 μL of metal-loaded MetAP to a 16 μL substrate−buffer mixture at 30 °C for 1 min. The reaction was quenched by the addition of 20 μL of 1% trifluoroacetic acid solution (TFA). Elution of the product was monitored at 215 nm following separation on a C8 HPLC column (Phenomenex, Luna; 5 μm, 4.6 × 25 cm), as previously described (*15*, *18*). The kinetic parameters v (velocity) and K_m (Michaelis constant) were determined in triplicate. Enzyme activities are expressed as units per milligram, where one unit is defined as the amount of enzyme that releases 1 μmol of product in 1 min at 30 °C. The metal binding titration and temperature dependence reactions were carried out using the same conditions as determined for the kinetic constants.

Isothermal Titration Calorimetry. Isothermal titration calorimetry (ITC) measurements were carried out on a MicroCal OMEGA ultrasensitive titration calorimeter. The titrant ($MnCl_2$ = 99.999%; Strem Chemicals, Newburyport, MA, or Aldrich) and sample solutions (apo-*Ec*MetAP-I or apo-*Pf*MetAP-II) were prepared in chelexed 25 mM Hepes buffer at pH 7.5 containing 150 mM KCl. Stock buffer solutions were thoroughly degassed before each titration. The enzyme solution (70 μM) was placed in the calorimeter cell and stirred at 200 rpm to ensure rapid mixing. Typically, 3 μL of titrant was delivered over 7.6 s with a 5 min interval between injections to allow for complete equilibration. Each titration was continued until 4.5−6 equiv of Mn(II) had been added to ensure that no additional complexes were formed in excess titrant. A background titration, consisting of the identical titrant solution but only the buffer solution in the sample cell, was subtracted from each experimental titration to account for heat of dilution. The data were analyzed with a two-site binding model by the Windows-based Origin software package supplied by MicroCal.

X-ray Absorption Spectroscopy of EcMetAP-I. EXAFS samples of *Ec*MetAP-I (1 mM) with 1 or 2 equiv of added Mn(II) (i.e., [Mn(II)_(*Ec*MetAP-I)] and [Mn(II)Mn(II)-(*Ec*MetAP-I)]) were prepared in chelexed 25 mM Hepes buffer at pH 7.5 containing 150 mM KCl with 5% glycerol. For Mn(II)-loaded *Ec*MetAP-I, EXAFS samples were frozen in polycarbonate cuvettes, 24 × 3 × 1 mm, with a 0.025 mm Mylar window covering one 24 × 3 mm face. XAS data were collected at the Stanford Synchrotron Radiation Laboratory (SSRL) with the SPEAR storage ring operating at 3.0 GeV (Table 1). The edge regions for multiple scans obtained on the same sample were compared to ensure

Table 1: X-ray Absorption Spectroscopic Data Collection

	Mn EXAFS
SR facility	SSRL
beamline	7-3
current in storage ring, mA	80−100
monochromator crystal	Si[220]
detection method	fluorescence
detector type	solid state array[a]
scan length, min	28
scans in average	16
temperature, K	10
energy standard	Mn foil, first inflection
energy calibration, eV	6539
E_0, eV	6545
preedge background	
energy range, eV	6215−6500
Gaussian center, eV	5898
width, eV	800
spline background	
energy range, eV	6545−6730 (4)
(polynomial order)	6730−6915 (4)

[a] The 13-element Ge solid-state X-ray fluorescence detector at SSRL is provided by the NIH Biotechnology Research Resource.

that the sample was not damaged by exposure to X-ray radiation. EXAFS analysis was performed using EXAFSPAK software (www-ssrl.slac.stanford.edu/exafspak.html) according to standard procedures (*21*). Multiple-scattering analysis was performed as described previously (*19*). Both single- and multiple-scattering paths of 4.5 Å from the Mn atom were used to identify and quantify imidazole coordination due to histidine. Multiple-scattering models, calculated using FEFF v7 (*23*), were based on hexaimidazole manganese(II) chloride tetrahydrate (*24*). Possible coordination numbers of histidyl imidazole ligands were chosen from fits that yielded chemically and physically reasonable Debye−Waller factors for the outer-shell atoms, since goodness-of-fit values (f') were relatively insensitive to these coordination numbers.

RESULTS

Time Dependence of Mn(II) Binding and Mn(II) Content of EcMetAP-I and PfMetAP-II. The time required to fully activate either *Ec*MetAP-I or *Pf*MetAP-II with Mn(II) ions was measured (Figure 1). For *Ec*MetAP-I, no change in the specific activity was observed even with incubation times as short as 10 min. However, for *Pf*MetAP-II, fully active enzyme was not obtained until after 90 min had passed. Therefore, all kinetic and metal binding measurements for *Pf*MetAP-I were made after a 90 min incubation period. Interestingly, Fe(II) and Co(II) activate *Pf*MetAP-II in 10 min, similar to *Ec*MetAP-I. The number of tightly bound Mn(II) ions was determined for *Ec*MetAP-I and *Pf*MetAP-II by ICP-AES analysis. MetAP samples (30 μM), to which 2−30 equiv of Mn(II) was added, were dialyzed extensively for 3 h at 4 °C against metal-free Hepes buffer. Upon ICP-AES analysis 1.3 and 1.5 ± 0.1 equiv of manganese was found coordinated to *Ec*MetAP-I and *Pf*MetAP-II, respectively. These data suggest that one Mn(II) ion is tightly bound to both *Ec*MetAP-I and *Pf*MetAP-II at these enzyme concentrations, while the second metal ion is partially labile on the time scale of the buffer exchange (3 h, 4 °C).

Determination of the K_m Values for MAS and MGMM. The strength of MAS and MGMM binding to the active site of Mn(II)-loaded *Ec*MetAP-I and *Pf*MetAP-II was determined (Table 2). The initial rates of hydrolysis of MAS or MGMM by Mn(II)-loaded *Ec*MetAP-I and *Pf*MetAP-II were monitored as a function of AS or GMM concentration, respectively, in 25 mM Hepes buffer, pH 7.5, and 150 mM KCl. Triplicate activity assay determinations at six concentrations of MAS or MGMM (0−9 mM) were made and the results plotted as $1/v$ vs 1/[S]. From fits of these data, the Michaelis constant (K_m) for MAS and MGMM binding to Mn(II)-loaded *Ec*MetAP-I and *Pf*MetAP-II was determined (Table 2). For Mn(II)-loaded *Ec*MetAP-I, no catalytic turnover was observed in the presence of MAS even at substrate concentrations of 20 mM while Mn(II)-loaded *Pf*MetAP-II bound MAS weakly (K_m = 5.7 mM). Similarly, k_{cat} values were determined for Mn(II)-loaded *Pf*MetAP-II toward both substrates and *Ec*MetAP-I toward MGMM. A 16-fold decrease in k_{cat} was observed for Mn(II)-loaded *Pf*MetAP-II toward MAS vs MGMM. This decrease in k_{cat} results in a decrease in the catalytic efficiency (k_{cat}/K_m) of over 60-fold. Interestingly, at 30 °C Mn(II)-loaded *Ec*MetAP-I exhibits a turnover rate that is more than 13 times faster than Mn(II)-loaded *Pf*MetAP-II toward MGMM. Since the K_m values are similar for the two enzymes toward MGMM, Mn(II)-loaded *Ec*MetAP-I is a better catalyst by 16-fold. On the other hand, at 85 °C, the optimum temperature for catalytic activity for Mn(II)-loaded *Pf*MetAP-II, the k_{cat} value increases 5-fold to164 s^{-1}, but the K_m value also

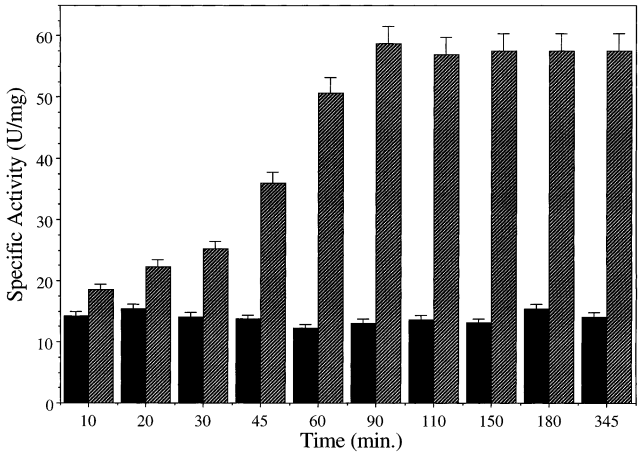

FIGURE 1: Plot of specific activity (units/mg) vs time. The solid bars represent activities obtained for Mn(II)-loaded *Ec*MetAP-I, and the shaded bars are activity levels observed for Mn(II)-loaded *Pf*MetAP-II. All activity measurements were performed at 30 °C, and all stock solutions were prepared anaerobically in 25 mM Hepes buffer at pH 7.5 containing 150 mM KCl. Each point represents the mean of three independent measurements.

Table 2: Kinetic Constants for Mn(II)-Loaded *Ec*MetAP-I and *Pf*MetAP-II for Various Substrates at 30 °C and pH 7.5

enzyme	kinetic constants	MGMM	MAS
Mn-*Ec*MetAP-I	K_m (mM)	1.3 ± 0.2	NR[a]
	k_{cat} (s^{-1})	4.6	
	k_{cat}/K_m (M^{-1} s^{-1})	3500	
	V_{max} (nmol min^{-1})	12.9 ± 0.4	
	SA (units/mg)	13 ± 2	
Mn-*Pf*MetAP-II	K_m (mM)	1.6 ± 0.2	5.7 ± 0.2
	k_{cat} (s^{-1})	32 ± 4	1.96
	k_{cat}/K_m (M^{-1} s^{-1})	20800	344
	V_{max} (nmol min^{-1})	155 ± 5	2.4 + 0.3
	SA (units/mg)	59 ± 5	3.6 ± 0.8

[a] No reaction was detected.

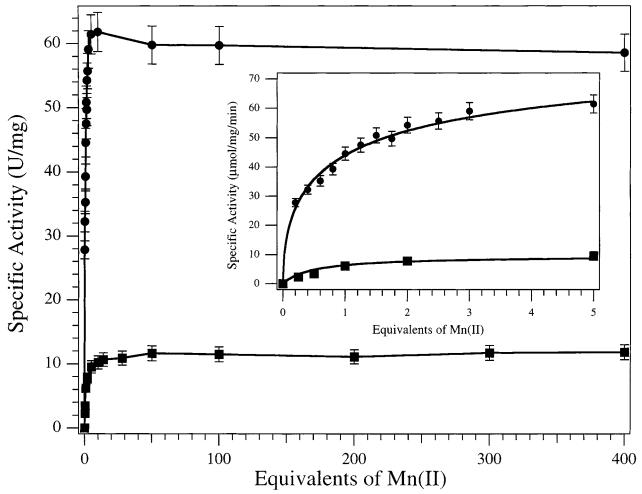

FIGURE 2: Plot of specific activity vs Mn(II) concentration (inset: expanded view of the 0−10 equiv region). All activity measurements were performed at 30 °C, and all stock solutions were prepared anaerobically in 25 mM Hepes buffer at pH 7.5 containing 150 mM KCl. Each point represents the mean of three independent measurements.

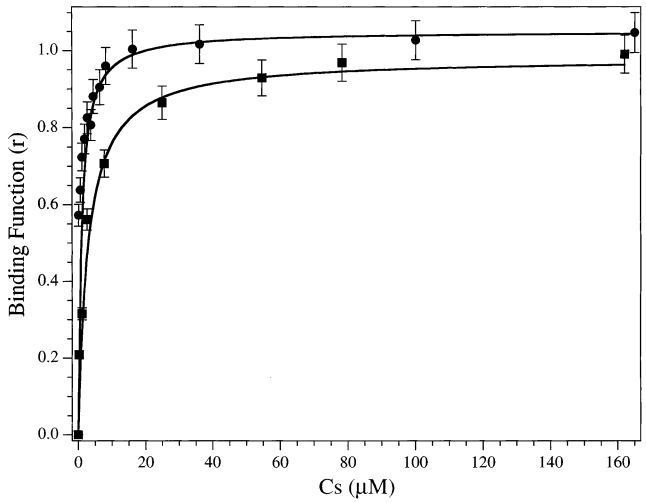

FIGURE 3: Plot of binding function, r, vs C_s (the concentration of free metal ions in solution) for Mn(II) titration into *Pf*MetAP-II (●) and *Ec*MetAP-I (■). The solid lines represent fits of the activity data to eq 1. Enzyme concentrations were 8.3 μM, and the measurements were made at 30 °C in 25 mM Hepes buffer, pH 7.5, and 150 mM KCl.

increases over 6-fold to 10.3 mM, resulting in a catalytic efficiency of 15900 M^{-1} s^{-1}, a 1.3-fold decrease.

Activity as a Function of Manganese(II) Concentration. The extent of hydrolytic activity exhibited by *Ec*MetAP-I and *Pf*MetAP-II was determined as a function of Mn(II) concentration. Apo-*Ec*MetAP-I and apo-*Pf*MetAP-II (both at 8.3 μM) were incubated with varying amounts of Mn(II), and the level of catalytic activity was determined (Figure 2). Upon the addition of Mn(II) to apo-*Ec*MetAP-I or apo-*Pf*MetAP-II under anaerobic conditions, the specific activity increased as a function of metal ion concentration up to approximately 2 equiv of Mn(II) for both *Ec*MetAP-I and *Pf*MetAP-II (Figure 2, inset). Further additions of up to 5 equiv of Mn(II) to either enzyme had little or no effect on the observed enzymatic activity. Interestingly, upon the addition of Mn(II) up to >830 μM (~100 equiv) the activity level of both enzymes remained constant and continued to remain constant even up to 400 equiv of added Mn(II) (Figure 2).

The activity titration data for Mn(II) binding to *Ec*MetAP-I and *Pf*MetAP-II (Figure 3) were fit to the equation (*24*):

$$r = pC_S/(K_d + C_S) \quad (1)$$

where p is the number of sites for which interaction with M(II) is governed by the intrinsic dissociation constant K_d and r is the binding function which was calculated as previously described (*14*). A value for the dissociation constants (K_d) was obtained by fitting these data via an iterative process that allowed both K_d and p to vary (Figure 3). The best fits obtained provided p values of 1 for both *Ec*MetAP-I and *Pf*MetAP-II with K_d values of 6 ± 0.5 and 1 ± 0.5 μM for Mn(II)-loaded *Ec*MetAP-I and *Pf*MetAP-II, respectively. Attempts to fit these data with a p value of 2 provided no improvements in the overall goodness of the fit.

Isothermal Titration Calorimetry. Isothermal titration calorimetry (ITC) measurements were carried out on a MicroCal OMEGA ultrasensitive titration calorimeter at 20 ± 0.2 °C for *Ec*MetAP-I and 30 ± 0.2 °C for *Pf*MetAP-II

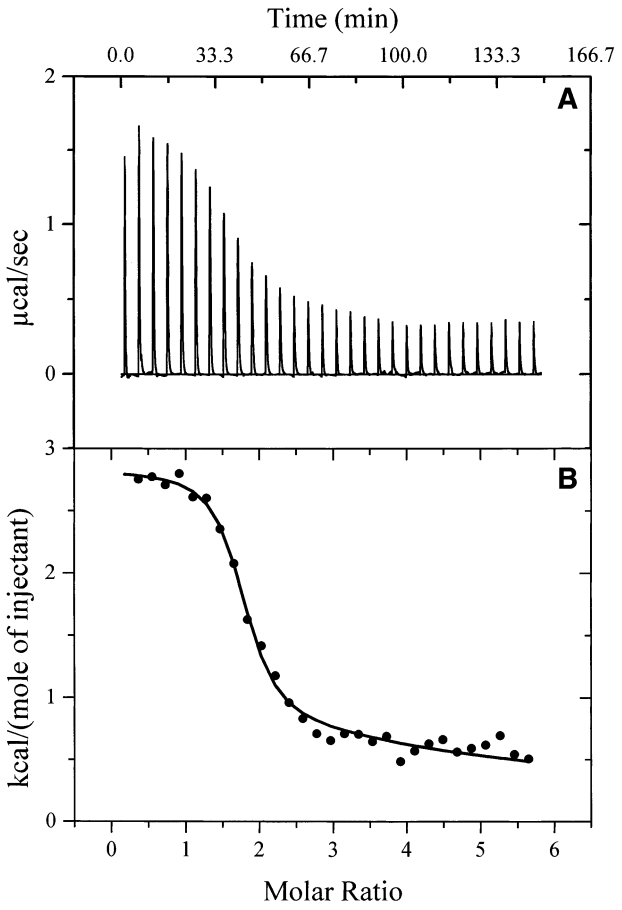

FIGURE 4: ITC titration of a 70 μM solution of *Ec*MetAP-I with a 5 mM Mn(II) solution at 20 °C in 25 mM Hepes buffer, pH 7.5, and 150 mM KCl.

(Figures 4A and 5A). Association constants (K_b) were obtained by fitting these data, after subtraction of the background heat of dilution, via an iterative process using the Origin software package. This software package uses a nonlinear least-squares algorithm which allows the concentrations of the titrant and the sample to be fit to the heat

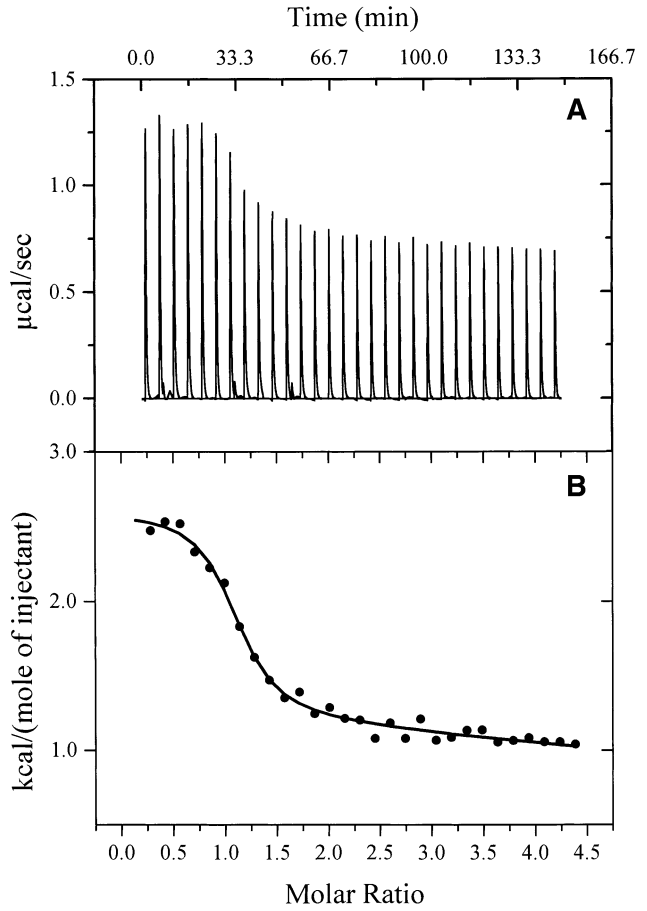

FIGURE 5: ITC titration of a 70 μM solution of *Pf*MetAP-II with a 5 mM Mn(II) solution at 30 °C in 25 mM Hepes buffer, pH 7.5, and 150 mM KCl.

flow per injection to an equilibrium binding equation for two sets of noninteracting sites. The K_b value, the enzyme−metal stoichiometry (*n*), and the change in enthalpy ($\Delta H°$) were allowed to vary during the fitting process. The best fits obtained for both *Ec*MetAP-I and *Pf*MetAP-II provided an overall *n* value of 3 for three noninteracting sites (Figures 4B and 5B). Attempts to fit these data with *n* values of 1 or 2 provided poor fits as did fits in which the *n* value was 3 but the binding process was considered cooperative. For *Ec*MetAP-I, a K_d value of 3.0 ± 0.2 μM was observed, and two K_d values of 4400 ± 300 μM were also obtained. On the other hand, a K_d value of 1.4 ± 0.2 μM was obtained for *Pf*MetAP-II, and two K_d values of 500 ± 50 μM were also obtained. These data correspond to individual binding events of three Mn(II) ions to the *Ec*MetAP-I and *Pf*MetAP-II enzymes.

Temperature Dependence of the Hydrolysis of MGMM by Mn(II)-Loaded PfMetAP-II. Mn(II)-loaded *Pf*MetAP-II was found to have optimal catalytic activity toward MGMM at 85 °C in 25 mM Hepes, pH 7.5, and 150 mM KCl buffer. Therefore, hydrolysis of MGMM was measured in triplicate between 25 and 85 °C at eight substrate concentrations ranging from 2 to 20 mM. From these data, K_m values were derived by fitting the experimental data to the Michaelis−Menten equation at each temperature studied (Figure 6B). The calculated specific activity values were plotted as a function of temperature between 25 and 85 °C (Figure 6A). The K_m and specific activity values for MGMM hydrolysis

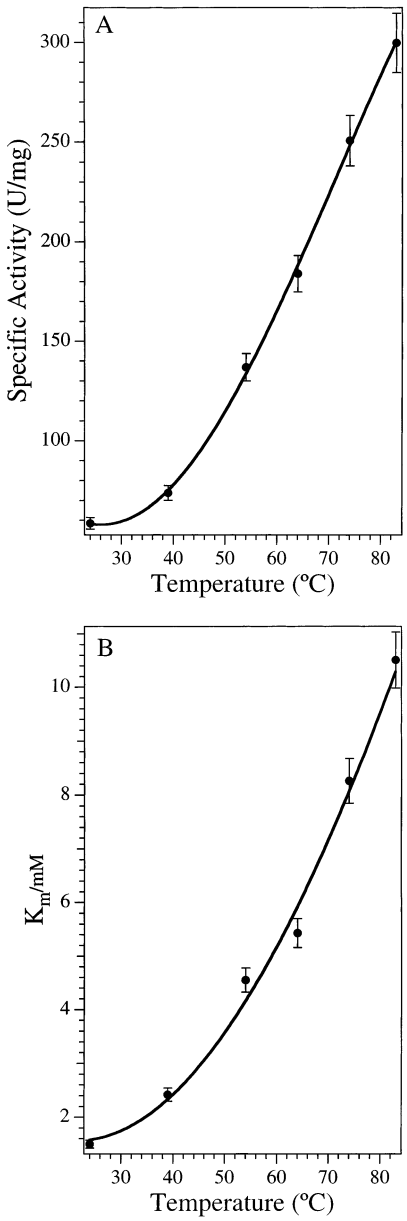

FIGURE 6: (A) Plot of specific activity (units/mg) of Mn(II)-loaded (●) *Pf*MetAP-II vs temperature between 25 and 85 °C. Each data point is the sum of three activity measurements at pH 7.5 in 25 mM Hepes buffer and 150 mM KCl at substrate concentrations ranging from 2 to 20 mM. (B) K_m vs temperature (°C).

catalyzed by Mn(II)-loaded *Pf*MetAP-II were found to increase with increasing temperature. *Pf*MetAP-II was stable at 85 °C for approximately 30 min before any loss in the enzymatic activity was detected. However, any loss in enzymatic activity was fully reversible, determined by V_{max}, for temperatures up to 70 °C. These data are very unusual since most enzymes undergo some denaturation at temperatures above 50 °C resulting in a decrease in V_{max} (*25*).

Since the enzyme concentration was not altered over the course of the experiment, an Arrhenius plot was constructed by plotting ln k_{cat} vs $1/T$ (Figure 7). A linear plot was obtained, indicating that the rate-limiting step does not change as the temperature is increased (*25*). From the slope of the line the activation energy, E_a, for temperatures between 296 and 358 K was calculated to be 25.7 kJ/mol for Mn(II)-loaded *Pf*MetAP-II. Since the slope of an Arrhenius plot is

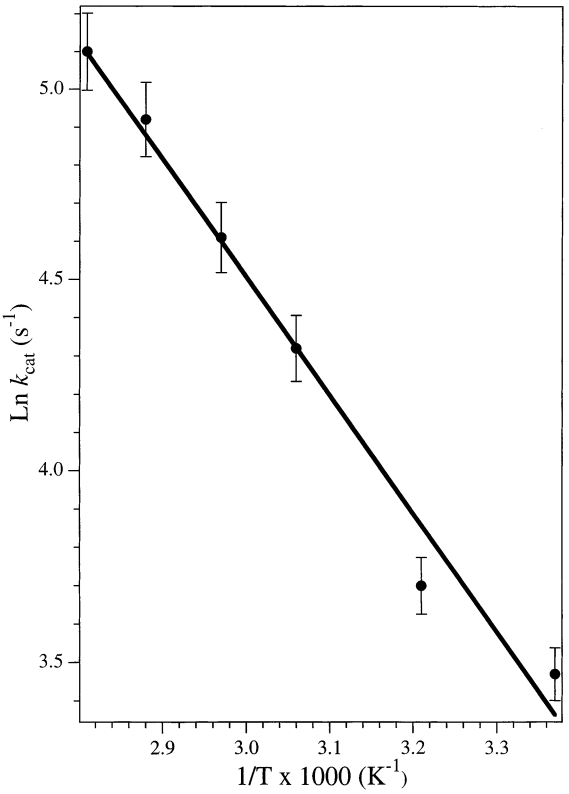

FIGURE 7: Arrhenius plot of ln k_{cat} vs $1/T$ for Mn(II)-loaded (●) *Pf*MetAP-II. The solid line is a direct fit to the Arrhenius equation.

equal to $-E_{a1}/R$, where $R = 8.3145$ J·K^{-1}·mol^{-1}, other thermodynamic parameters were calculated by the relations $\Delta G^{\ddagger} = -RT \ln(k_{cat}h/k_BT)$, $\Delta H^{\ddagger} = E_a - RT$, and $\Delta S^{\ddagger} = (\Delta H^{\ddagger} - \Delta G^{\ddagger})/T$, where k_B, h, and R are the Boltzmann, Planck, and gas constants, respectively, and were found to be $\Delta G^{\ddagger} = 50.1$ kJ/mol, $\Delta H^{\ddagger} = 23.2$ kJ/mol, and $\Delta S^{\ddagger} = -90.2$ J·mol^{-1}·K^{-1}.

X-ray Absorption Spectroscopy of EcMetAP-I. Manganese K-edge X-ray absorption (XAS) spectra were acquired on 1 mM samples of *Ec*MetAP-I with 1 or 2 equiv of added Mn(II) (i.e., [Mn(II)_(*Ec*MetAP-I)] and [Mn(II)Mn(II)-(*Ec*MetAP-I)]). For [Mn(II)Mn(II)(*Ec*MetAP-I)], the EXAFS data reveal an average of both metal ion environments. The 1s → 3d preedge transitions for each sample occur at 6540 eV (Figure 8). Since 1s → 3d preedge transitions are Laporte forbidden in centrosymmetric environments (e.g., octahedral but not tetrahedral), the intensity of the 1s → 3d preedge transition is inversely proportional to coordination number. The intensities of the observed transitions for all three samples are consistent with, on average, five- or six-coordinate Mn(II) sites.

Fourier transforms (FTs) of the EXAFS data for both samples are dominated by a peak at ca. 2.1 Å (Figure 9, bottom). Excellent single-shell fits of EXAFS spectra for both [Mn(II)_(*Ec*MetAP-I)] and [Mn(II)Mn(II)(*Ec*MetAP-I)] were obtained with 5 or 6 N/O scatterers at 2.15 Å (fits 1−3 and 6−8; Table 3). Attempts to include a Mn−Mn interaction in the 2.4−4.0 Å range in the curve fitting parameters were unsuccessful. Inclusion of multiple-scattering contributions from the outer-shell atoms of a histidine imidazole ring resulted in reasonable Debye−Waller factors and a slight reduction in the goodness-of-fit value (f') for [Mn(II)_(*Ec*MetAP-I)] (cf. fits 2 and 4; Table 3). If a second histidine imidazole ring was included in fits for [Mn(II)_(*Ec*MetAP-I)], the Debye−Waller factor values are significantly higher (fit 5; Table 3). For [Mn(II)Mn(II)(*Ec*MetAP-I)], inclusion of a single outer-shell histidine scatterer resulted in a Debye−Waller factor that is similar in magnitude to those obtained

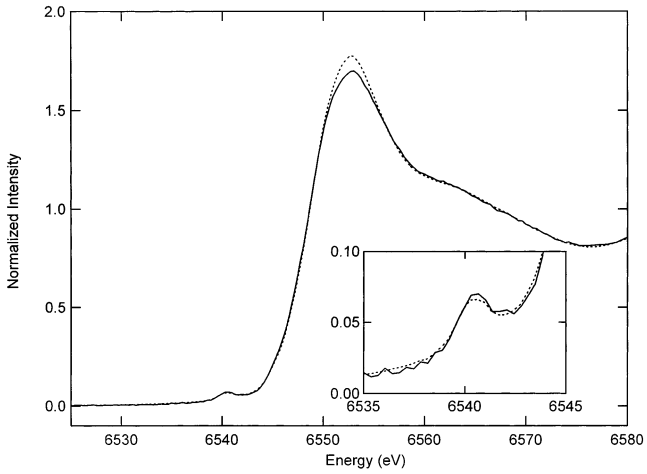

FIGURE 8: X-ray absorption K-edge spectra for *Ec*MetAP-I: [Mn(II)_(*Ec*MetAP-I)] (solid) and [Mn(II)Mn(II)(*Ec*MetAP-I)] (dotted). In the inset, the preedge 1s → 3d transition is expanded.

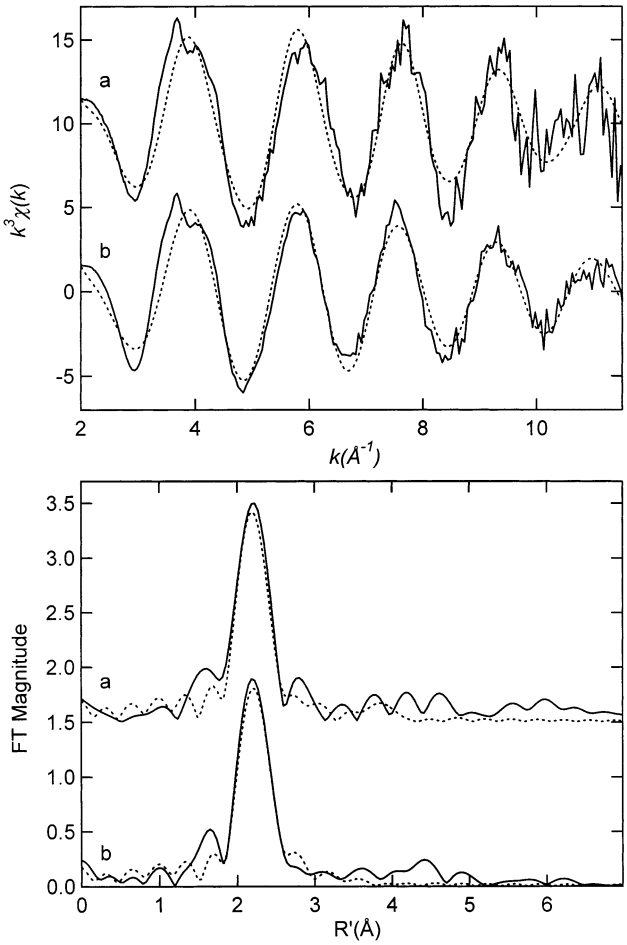

FIGURE 9: k^3-weighted Mn EXAFS (top) and Fourier transforms (bottom, over $k = 2-11.5$ Å^{-1}) for [Mn(II)_(*Ec*MetAP)] (a; solid) and the calculated spectra for Mn−O_5(imid) (dotted; fit 4, Table 2) and for [Mn(II)Mn(II)(*Ec*MetAP-I)] (b; solid) and the calculated spectra for Mn−O_6 (dotted; fit 7, Table 2).

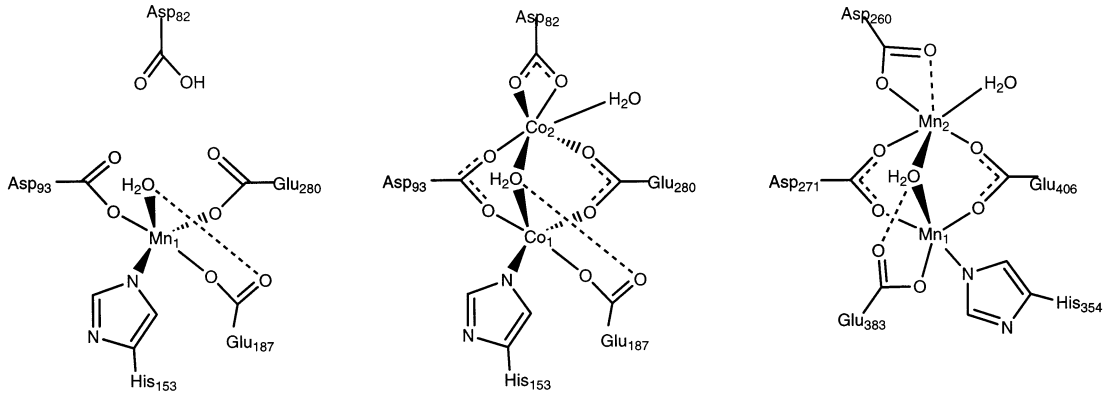

FIGURE 10: Drawing of the proposed active site of Mn(II)-loaded *Pf*MetAP-II or *Ec*MetAP-I compared to the X-ray crystallographically characterized dicobalt form of *Pf*MetAP-II and the dimanganese form of aminopeptidase P from *E. coli*.

Table 3: Curve Fitting Results for Mn-Loaded *Ec*MetAP-I EXAFS[a]

sample	fit	shell	R_{as} (Å)	σ_{as}^2 (Å^2)	ΔE_0 (eV)	f' [b]
[Mn(II)_(*Ec*MetAP-I)]	1	Mn−O_5	2.15	0.0044	−1.32	0.120
MM20A (2−11.5 Å^{-1})	2	Mn−O_6	2.15	0.0058	−1.68	0.114
$\Delta k^3\chi = 12.26$	3	Mn−O_7	2.15	0.0071	−1.94	0.113
	4	Mn−$(O,N)_6$	2.15	0.0058	−1.89	0.111
		Mn−C_{imid}	2.91	0.0036		
		Mn−C_{imid}	[3.01]	[0.0037]		
		Mn−N_{imid}	[3.98]	[0.0049]		
		Mn−C_{imid}	[4.03]	[0.0049]		
	5	Mn−$(O,N)_6$	2.15	0.0058	−1.95	0.110
		Mn−$(C_{imid})_2$	2.93	0.0096		
		Mn−$(C_{imid})_2$	[3.02]	[0.0100]		
		Mn−$(N_{imid})_2$	[4.00]	[0.0132]		
		Mn−$(C_{imid})_2$	[4.06]	[0.0132]		
[Mn(II)Mn(II)(*Ec*MetAP-I)]	6	Mn−O_5	2.16	0.0047	−1.51	0.082
MM22A (2−11.5 Å^{-1})	7	Mn−O_6	2.16	0.0062	−1.61	0.075
$\Delta k^3\chi = 11.82$	8	Mn−O_7	2.16	0.0076	−1.64	0.075
	9	Mn−$(O,N)_6$	2.16	0.0062	−1.57	0.071
		Mn−C_{imid}	2.97	0.0095		
		Mn−C_{imid}	[3.07]	[0.0099]		
		Mn−N_{imid}	[4.05]	[0.0131]		
		Mn−C_{imid}	[4.11]	[0.0131]		

[a] Group is the chemical unit defined for the multiple scattering calculation. N_s is the number of scatterers (or groups) per metal. R_{as} is the metal-scatterer distance. σ_{as}^2 is a mean square deviation in R_{as}. ΔE_0 is the shift in E_0 for the theoretical scattering functions. Numbers in brackets were constrained either to be a multiple of the above value (σ_{as}^2) or to maintain a constant difference from the above value (R_{as}, ΔE_0). [b] f' is defined as follows (chi-squared): $f' = \{?_i[k^3(\chi_i^{obs} - \chi_i^{calc})]^2/N_?^{?\ 1/2}\}/[(k^3\chi^{obs})_{max} - (k^3\chi^{obs})_{min}]$.

with two outer-shell histidine scatterers for [Mn(II)_(*Ec*MetAP-I)] (cf. fits 4, 5, and 9; Table 3). The Debye−Waller factor values are significantly higher for [Mn(II)-Mn(II)(*Ec*MetAP-I)] than [Mn(II)_(*Ec*MetAP-I)], consistent with the first Mn(II) ion binding to the histidine-containing site.

DISCUSSION

Until recently, all MetAP's studied have been reported to be Co(II)-dependent metalloproteases (*16*, *17*). This conclusion was arrived at from the reproducible observations that MetAP's show high activity in the presence of Co(II) when compared to the activity levels of other divalent metal ions such as Zn(II), Cu(II), or Ni(II). However, in all in vitro studies to date, Co(II) concentrations were artificially inflated to the millimolar range during purification. Walker and Bradshaw were the first to suggest that MetAP's could be activated by Zn(II) ions on the basis of activity measurements made on the type I MetAP from *S. cerevisiae* (*26*); however, *Ec*MetAP-I and more recently *Pf*MetAP-I and *Hs*MetAP-II were shown to be inactive in the presence of Zn(II), but each of these enzymes is fully active in the presence of 1 equiv of Co(II) while *Ec*MetAP-I and *Pf*MetAP-II are equally as active in the presence of 1 equiv of Fe(II) (*18*). On the other hand, *Ec*MetAP-I was found to retain 30% of the observed Co(II) activity in the presence of excess Mn(II) (*18*). Iron, manganese, and zinc, unlike cobalt, are abundant in nature and have many known biological roles (*27*). The question of what type and how many divalent metal ions are required to activate MetAP's is of particular importance since MetAP's are currently under heavy investigation as anti-angiogenesis targets for anticancer drugs. To design and synthesize small molecule drug candidates with nanomolar or picomolar binding constants to MetAP's, the number, geometry, and type of in vivo metal ions must be elucidated.

The evidence suggesting that a single Fe(II) ion is required to activate all MetAP's is growing but has yet to be unequivocally proven. Since Mn(II) ions can also activate

MetAP's, we have investigated the enzymatic activity of Mn(II)-loaded *Ec*MetAP-I and *Pf*MetAP-II. Activity measurements as a function of added Mn(II) show that both *Ec*MetAP-I and *Pf*MetAP-II are maximally stimulated upon the addition of 2 equiv of metal ion. The addition of up to 400 equiv of Mn(II) did not significantly change the observed catalytic activity levels. In addition, ICP-AES analyses of 30 μM Mn(II)-loaded *Ec*MetAP-I and *Pf*MetAP-II samples that had been extensively dialyzed against metal-free buffer routinely indicated that 1.3 and 1.5 equiv of divalent metal ions are tightly bound per enzyme molecule to *Ec*MetAP-I and *Pf*MetAP-II, respectively. These data suggest that at least one Mn(II) ion is tightly bound to both enzymes while a second is more weakly bound and likely in equilibrium between a metal-bound and unbound form at these enzyme concentrations ($\sim$8 μM). Moreover, these data indicate that the monometal form of *Ec*MetAP-I and *Pf*MetAP-II is catalytically competent. To determine if a dinuclear site is formed at an enzyme concentration of $\sim$8 μM, the metal binding constants for both metal binding events were determined.

Fits of the titration data obtained for both *Ec*MetAP-I and *Pf*MetAP-II with Mn(II) ions provided dissociation constants (K_d) for the first metal binding site of 6 and 1 μM, respectively. Since only one metal ion is bound to the enzyme active site, these K_d values correspond to the microscopic binding constants for the binding of a single metal ion to *Ec*MetAP-I and *Pf*MetAP-II. Confirmation of these K_d values was obtained from isothermal titration calorimetry (ITC), which provided K_d values of 4.4 and 1.3 μM for Mn(II) binding to *Ec*MetAP-I and *Pf*MetAP-II, respectively. Further, the ITC data indicated that two additional Mn(II) ions can bind to both *Ec*MetAP-I and *Pf*MetAP-II with K_d values of 4400 and 500 μM, respectively. A second Co(II) ion has been shown to bind to *Ec*MetAP-I and *Pf*MetAP-II with K_d values of 2500 and 500 μM, respectively. Moreover, a third Co(II) ion binding site was identified in the X-ray crystal structure of *Ec*MetAP-I (*11*). On the basis of these data and those presented herein, only one Mn(II) ion is tightly bound to either *Ec*MetAP-I or *Pf*MetAP-II, and thus only one Mn(II) ion is needed to activate either enzyme. The fact that the catalytic activity does not plateau until more than 2 equiv of Mn(II) are added is because the K_d values for the first metal binding event is on the order of the enzyme concentration used in the experiment. Our data also suggest that the putative second metal ion in the active site of MetAP's and the third metal binding site have similar metal binding affinities.

The K_d values obtained for Mn(II) binding to *Ec*MetAP-I and *Pf*MetAP-II are somewhat weaker than those observed for Co(II) or Fe(II) *Ec*MetAP-I and *Pf*MetAP-II. For *Ec*MetAP-I and *Pf*MetAP-II, the K_d values for Co(II) binding were 300 and 50 nM while those for Fe(II) binding were 200 and 20 nM, respectively (*15*). The K_d values observed for Mn(II) binding to either *Ec*MetAP-I or *Pf*MetAP-II are approximately a factor of 5 weaker than Co(II) or Fe(II) binding to either enzyme. The observed K_d values for the first Mn(II) binding event to either *Ec*MetAP-I or *Pf*MetAP-II are also 10$-$100 times larger than the reported K_d values for several other hydrolytic enzymes that contain carboxylate-rich active sites. For example, the K_d values for the first metal binding site of the aminopeptidase from *Aeromonas proteolytica* is 1 nM (*28*), and the β-lactamase from *Bacillus cereus* has a divalent metal ion K_d value of 620 nM (*29*). On the other hand, the observed K_d values for Mn(II) binding to *Ec*MetAP-I or *Pf*MetAP-II are similar in magnitude to the K_d value reported for the Mn(II)-dependent clostridial aminopeptidase P (AMPP) of 7 μM, which has active site ligands identical to those of MetAP's (*30*).

Since *Pf*MetAP-II is stable at 75 °C for 1 h, *Pf*MetAP-II provides the unique opportunity to determine the activation parameters of the ES‡ complex over a wide temperature range. Construction of an Arrhenius plot from the temperature dependence of Mn(II)-loaded *Pf*MetAP-II activity indicates that the rate-limiting step does not change as a function of temperature and is product release (*25*). This finding is similar to that obtained for Co(II)- and Fe(II)-loaded *Pf*MetAP-II (*14*). The activation energy (E_a) for the activated ES‡ complex is 25.7 kJ/mol, which is nearly double the value obtained for either Co(II)- and Fe(II)-loaded *Pf*MetAP-II (*14*). The enthalpy of activation calculated over the temperature range 25$-$85 °C is 23.2 kJ/mol while the entropy of activation was found to be -90.2 J·mol^{-1}·K^{-1} at 25 °C. The positive enthalpy is indicative of a conformation change upon substrate binding, likely due to the energy of bond formation and breaking during nucleophilic attack on the scissile carbonyl carbon of the substrate. On the other hand, the large negative entropy value suggests that some of the molecular motions are lost upon ES‡ complex formation possibly due to hydrogen bond formation between catalytically important amino acids and the substrate. All of these factors contribute to the large positive free energy of activation of 50.1 kJ/mol. Interestingly, the observed specific activity of Mn(II)-loaded *Pf*MetAP-II increases from $\sim$60 to 300 units/mg between 25 and 85 °C. The specific activity observed for Mn(II)-loaded *Pf*MetAP-II at 85 °C is roughly equal to the specific activity of Co(II)- and Fe(II)-loaded *Pf*MetAP-II at 25 °C but is still $\sim$3 times lower than the activity levels obtained at 85 °C. However, the K_m value for Mn(II)-loaded *Pf*MetAP-II also increases to over 10 mM at 85 °C so the catalytic efficiency of Mn(II)-loaded *Pf*MetAP-II does not change significantly over this temperature range. On the basis of these data, Fe(II)-loaded *Pf*MetAP-II is a much better catalyst at the optimum growth temperature of *P. furiosus* (85 °C) than either Co(II)- or Mn(II)-loaded *Pf*MetAP-II (*14*). These data further suggest that Fe(II) is the physiologically relevant metal ion.

Since Mn(II)-loaded *Ec*MetAP-I and *Pf*MetAP-II are colorless and no X-ray structural data have been reported, the structural aspects of these catalytically competent MetAP enzymes are unknown. Therefore, extended X-ray absorption fine structure (EXAFS) data were recorded on [Mn(II)$_2$(*Ec*MetAP-I)] and [Mn(II)Mn(II)(*Ec*MetAP-I)] and provide the first structural glimpse of the Mn(II) active sites of *Ec*MetAP-I. The EXAFS data are consistent with the X-ray crystal structure of Co(II)-loaded *Ec*MetAP-I, which indicates that the histidine-ligated Co(II) ion resides in a distorted trigonal-bipyramidal coordination environment made up of oxygen or nitrogen donor ligands while the second Co(II) ion is also trigonal bipyramidal (*12*, *31*). The average bond distances obtained by EXAFS for both *Ec*MetAP-I samples are in good agreement with the crystallographically determined bond lengths for [Co(II)Co(II)(*Ec*MetAP-I)] of 2.04 Å (*12*). Additionally, it was recently reported, on the basis

of ^{1}H NMR data, that upon the addition of Co(II) to *Ec*MetAP-I, the first Co(II) is bound to the lone histidine residue in the active site (*15*). This is consistent with the suggestion of a single histidine ligand at the active site, based on crystallographic analyses. The Debye−Waller factor values for the Mn−histidine interaction are significantly higher for [Mn(II)Mn(II)(*Ec*MetAP-I)] than for [Mn(II)_(*Ec*MetAP-I)], suggesting that the first Mn atom is located in the histidine-ligated site. Furthermore, the EXAFS data do not detect a Mn−Mn interaction similar to data obtained for [Co(II)Co(II)(*Ec*MetAP-I)] and [Fe(II)Fe(II)(*Ec*MetAP-I)] (*19*). These data indicate that a dinuclear Mn(II) site does not exist in *Ec*MetAP-I, as seen in the published X-ray crystal structures for all Co(II)-loaded MetAP's (*11*, *12*). The lack of a M−M FT peak in the second shell of [Mn(II)Mn(II)-(*Ec*MetAP-I)] is consistent with a single Mn(II) ion being capable of activating MetAP's and is also in line with the metal binding constants reported herein.

Biological and Mechanistic Implications. According to the recently proposed mechanism for the aminopeptidase from *A. proteolytica* (AAP), substrate binding to the hydrophobic pocket adjacent to the dinuclear active site is the first step in catalysis (*32*). Since a hydrophobic pocket is also adjacent to the metallo active site in all MetAP's, the first step in catalysis for MetAP's is likely similar to AAP. When substrate (MGMM) binds to MetAP, the carbonyl oxygen of the N-terminal methionine must be activated, probably by binding to the active site metal ion (*31*). Once carbonyl activation occurs, the nucleophilic hydroxide must be oriented correctly for attack on the scissile carbonyl carbon. For Zn(II)-loaded *Ec*MetAP-I and *Pf*MetAP-II, the correct positioning of the scissile carbonyl carbon must not occur for catalytic turnover since each of these enzymes is inactive in the presence of Zn(II). This may simply be the result of a trigonal-bipyramidal (TBP) geometry for Co(II), Fe(II), and Mn(II) bound in the first site of MetAP's vs a tetrahedral (T_d) or trigonal planar geometry if Zn(II) were bound instead (unpublished results). The proposal that Zn(II) prefers a T_d geometry comes from the ligand field stabilization energies (LFSE's) for octahedral (O_h), T_d, or trigonal planar geometries of Zn(II) and the observed X-ray crystal structure of Zn(II)-loaded *Pf*MetAP-II (unpublished results) and Zn(II) model complexes with mixed O/N ligands. For both O_h and T_d geometries, the LFSE's are zero, suggesting that neither structure is favored. However, on the basis of X-ray crystallographic data, Zn(II) clearly favors a T_d geometry (*33*). The reason for this is that the 4s and 4p orbitals are easily accessible as electron pair acceptors, providing an sp^3-type center, while the 4d orbitals are higher in energy, making the formation of O_h or trigonal-bipyramidal (TBP) complexes less favorable.

Another factor that might be involved in the catalytic process is the change in Lewis acidity between Co(II), Fe(II), or Mn(II) vs Zn(II). The effect of Lewis acidity on the reaction catalyzed by MetAP's can be gleaned from the k_{cat}/K_m values for Mn(II)-, Fe(II)-, and Co(II)-loaded forms of MetAP's determined at 30 °C. Toward the substrate MGMM, the k_{cat}/K_m values are 20800, 36900, and 30600 M^{-1} s^{-1} for Mn(II)-, Fe(II)-, and Co(II)-loaded *Pf*MetAP-II, respectively, and for Mn(II)-, Fe(II)-, and Co(II)-loaded *Ec*MetAP-I the k_{cat}/K_m values are 3500, 13700, and 12100 M^{-1} s^{-1}, respectively. These observations are consistent with the fact that Mn(II) is a harder acid than either Fe(II) or Co(II); however, the k_{cat}/K_m values do not change markedly with regard to the metal ion in the active site. Therefore, these data suggest that Lewis acidity is not the major factor for catalytic turnover to occur.

The proposal that a TBP geometry for the catalytic metal ion in the active site of MetAP's is required is also supported by the fact that when Cu(II) is substituted into *Ec*MetAP-I, it resides in a square-based pyramidal (SP) geometry, and the resulting enzyme is inactive. Moreover, Ni(II) cannot activate MetAP's, but for Ni(II), an O_h geometry is significantly favored over T_d or TBP geometries on the basis of LFSE's. These data, coupled with the fact that the vast majority of metalloproteases can be activated by every first row transition metal ion from Co(II) to Zn(II), suggest that the Lewis acidity of the metal ion bound in the active site of MetAP's is less important than the coordination geometry that the hydrolytic metal ion, M1, adopts. The geometrical importance of the catalytic metal ion in MetAP's is likely widely applicable to hydrolytic metalloenzymes with both mono- and dinuclear active sites. Thus, metal ion geometry is critical for the activated substrate and for the nucleophile to be positioned correctly for catalytic turnover to occur while Lewis acidity likely plays a secondary role to metal ion geometry.

REFERENCES

1. Bradshaw, R. A. (1989) *Trends Biochem. Sci. 14*, 276−279.
2. Meinnel, T., Mechulam, Y., and Blanquet, S. (1993) *Biochimie 75*, 1061−1075.
3. Bradshaw, R. A., Brickey, W. W., and Walker, K. W. (1998) *Trends Biochem. Sci. 23*, 263−267.
4. Arfin, S. M., and Bradshaw, R. A. (1988) *Biochemistry 27*, 7979−7984.
5. Hirel, P.-H., Schmitter, J.-M., Dessen, P., Fayat, G., and Blanquet, S. (1989) *Proc. Natl. Acad. Sci. U.S.A. 86*, 8247−8251.
6. Ben-Bassat, A., Bauer, K., Chang, S.-Y., Myambo, K., Boosman, A., and Chang, S. (1987) *J. Bacteriol. 169*, 751−757.
7. Chang, S.-Y. P., McGary, E. C., and Chang, S. (1989) *J. Bacteriol. 171*, 4071−4072.
8. Miller, C. G., Kukral, A. M., Miller, J. L., and Movva, N. R. (1989) *J. Bacteriol. 171*, 5215−5217.
9. Li, X., and Chang, Y.-H. (1995) *Proc. Natl. Acad. Sci. U.S.A. 92*, 12357−12361.
10. Tahirov, T. H., Oki, H., Tsukihara, T., Ogasahara, K., Yutani, K., Ogata, K., Izu, Y., Tsunasawa, S., and Kato, I. (1998) *J. Mol. Biol. 284*, 101−124.
11. Lowther, W. T., Orville, A. M., Madden, D. T., Lim, S., Rich, D. H., and Matthews, B. W. (1999) *Biochemistry 38*, 7678−7688.
12. Roderick, S. L., and Matthews, B. W. (1993) *Biochemistry 32*, 3907−3912.
13. Liu, S., Widom, J., Kemp, C. W., Crews, C. M., and Clardy, J. (1998) *Science 282*, 1324−1327.
14. Meng, L., Ruebush, S., D'souza, V. M., Copik, A. J., Tsunasawa, S., and Holz, R. C. (2002) *Biochemistry 41* (in press).
15. D'souza, V. M., Bennett, B., Copik, A. J., and Holz, R. C. (2000) *Biochemistry 39*, 3817−3826.
16. Barrett, A. J., Rawlings, N. D., and Woessner, J. F. (1998) pp 1−1666, Academic Press, London.
17. Taylor, A. (1996) in *Molecular Biology Intelligence Unit* (A., T., Ed.) pp 1−219, R. G. Landes Co., Austin, TX.
18. D'souza, V. M., and Holz, R. C. (1999) *Biochemistry 38*, 11079−11085.
19. Cosper, N. J., D'souza, V., Scott, R., and Holz, R. C. (2001) *Biochemistry 40*, 13302−13309.
20. Lowther, W. T., McMillen, D. A., Orville, A. M., and Matthews, B. W. (1998) *Proc. Natl. Acad. Sci. U.S.A. 95*, 12153−12157.
21. Scott, R. A. (1985) *Methods Enzymol. 117*, 414−458.
22. Cosper, N. J., Stalhandske, C. M. V., Saari, R. E., Hausinger, R. P., and Scott, R. A. (1999) *J. Biol. Inorg. Chem. 4*, 122−129.

23. Zabinski, S. I., Rehr, J. J., Ankudinov, A., Albers, R. C., and Eller, M. (1995) *J. Phys. Rev. B 11*, 305.
24. Garrett, T. P. J., Guss, J. M., and Freeman, H. C. (1983) *Acta Crystallogr. 39*, 1027.
25. Segel, I. H. (1975) *Enzyme Kinetics: Behavior and analysis of rapid equilibrium and steady-state enzyme systems*, 1st ed., John Wiley & Sons, New York.
26. Walker, K. W., and Bradshaw, R. A. (1998) *Protein Sci. 7*, 2684−2687.
27. Holm, R. H., Kennepohl, P., and Solomon, E. I. (1996) *Chem. Rev. 96*, 2239−2314.
28. Prescott, J. M., and Wilkes, S. H. (1976) *Methods Enzymol. 45B*, 530−543.
29. de Seny, D., Heinz, U., Wommer, S., Kiefer, M., Meyer-Klaucke, Galleni, M., Frere, J.-M., Bauer, R., and Adolph, H.-W. (2001) *J. Biol. Chem. 276*, 45065−45078.
30. Fleminger, G., and Yaron, A. (1984) *Biochim. Biophys. Acta 789*, 245−256.
31. Lowther, T. W., Zhang, Y., Sampson, P. B., Honek, J. F., and Matthews, B. W. (1999) *Biochemistry 38*, 14810−14819.
32. Stamper, C., Bennett, B., Edwards, T., Holz, R. C., Ringe, D., and Petsko, G. (2001) *Biochemistry 40*, 7034−7046.
33. Bertini, I., Luchinat, C., Rosi, M., Sgamellotti, A., and Tarantelli, F. (1990) *Inorg. Chem. 29*, 1460−1463.

BI020395U